Journal of Analytical and Applied Pyrolysis 171 (2023) 105973

Contents lists available at ScienceDirect

Journal of Analytical and Applied Pyrolysis

journal homepage: www.elsevier.com/locate/jaap

A study on the impact of the reaction mechanism of the thermochemical activation of bone char (by pyrolysis and carbonization)

Irene Sierra [a,*], José L. Ayastuy [b], Miguel A. Gutiérrez-Ortiz [b], Unai Iriarte-Velasco [a]

[a] Department of Chemical Engineering, Faculty of Pharmacy, University of the Basque Country UPV/EHU, Paseo de la Universidad 7, 01006 Vitoria-Gasteiz, Spain
[b] Department of Chemical Engineering, Faculty of Science and Technology, University of the Basque Country UPV/EHU, Barrio Sarriena s/n, 48940 Leioa, Spain

ARTICLE INFO

Keywords:
Bioapatite
Bone char
Activation mechanism
Mass spectrometry
H_2SO_4
K_2CO_3

ABSTRACT

Porous materials based on bioapatite were prepared through the thermochemical activation of pork bone char, using different reagents (H_2SO_4 and K_2CO_3), heating atmosphere (inert and oxidizing) and activation temperature. Thermogravimetric analysis coupled to mass spectrometry was used to propose a detailed activation mechanism. Regarding the effect of each reagent on the activation, whereas that of H_2SO_4 is attributed to specific reactions, the effect of K_2CO_3 is ascribed to (i) the role of K^+ as a catalyst for reactions such as the gasification of carbon and (ii) the incorporation of carbonates, involved in several reactions. The best textural properties are obtained in an oxidizing atmosphere at 350 ºC. The beneficial effect of the combustion reactions at an intermediate temperature results in a cost-effective preparation protocol. H_2SO_4 leads to a selective development of microporosity. The oxidizing atmosphere is involved in the generation of OH^- functional groups. These results demonstrate the feasibility of configuring activation protocols to tailor the physicochemical properties of biapatite-based materials, for use in specific fields.

1. Introduction

There is a growing interest in materials that fall into the calcium phosphate spectrum. Among them, hydroxyapatite (HAp), $[Ca_{10}(PO_4)_6(OH)_2]$ is one of the most promising. HAp, a mineral form of calcium phosphate, is a versatile material due to its structural stability, acid–base properties and ionic substitution ability. Hydroxyapatite can be chemically synthesized using various procedures such as precipitation, hydrolysis, sol–gel approach, hydrothermal, emulsion, dry methods and mechanochemical synthesis [1]. In the configuration of materials based on HAp, the use of natural bio-resources such as waste animal bones is a promising choice among the possible options, since bioapatite is the main inorganic component of bones.

The global slaughter industry produces billions of kg of animal bone residues every year. The use of meat and bone meal (MBM) to feed cattle was forbidden in EU (Commission Decision 94/381/EC), as a result of the bovine spongiform encephalopathy crisis. Consequently, there is a high amount of animal wastes that must be safely disposed or transformed. The development of an adequate technology for the conversion of waste material into value-added products will help overcome this growing challenge. The thermochemical conversion of waste animal bones can be used to produce porous materials. Thus, one of the advantages of this strategy is the reduction of the high amount of animal wastes to be safely disposed, with the corresponding environmental benefit. The solid produced contains mainly biological apatite, a ramification of hydroxyapatite.

Materials based on hydroxyapatite have been used in several fields such as the removal of pollutants from liquid and gaseous streams [2–5], in catalytic systems [6], in electrochemistry [6,7] and in biomedical applications [8,9]. Consequently, the production of porous materials from waste animal bones, an abundant and available low-cost material, could be economically feasible as well as environmentally friendly.

The potential applications of these materials are closely related to their physicochemical properties such as specific surface area, porosity, Ca/P molar ratio, phase composition and particle size [10]. For example, a nanocrystalline HAp with high surface area and small particle size can offer an adequate sorption capacity and cell compatibility to be applied as adsorbent and biomaterial [11]. Thus, if adequate treatment methods are developed, the use of animal bones could represent a promising alternative for the production of bioapatite-based porous materials with tailored properties.

Thermal treatment constitutes one of the most reliable treatment

* Corresponding author.
E-mail address: irene.sierra@ehu.eus (I. Sierra).

https://doi.org/10.1016/j.jaap.2023.105973
Received 9 February 2023; Received in revised form 29 March 2023; Accepted 9 April 2023
Available online 10 April 2023

methods for the residual animal bones. The solid fraction obtained, containing mainly biological apatite, is referred to as bone char. The physicochemical properties of this material can be enhanced by chemical activation. The chemical activation of biomass precursors has several advantages over physical activation: (i) higher yield, (ii) lower activation temperatures required, (iii) less time required in the activation process, (iv) possibility of incorporating suitable functional groups, (v) better development of the porous structure, and (vi) higher surface area [12]. The most commonly used reagents for chemical activation include inorganic salts (e.g. K_2CO_3), alkali hydroxides (KOH, NaOH), as well as inorganic acids (such as H_2SO_4 and H_3PO_4) [13,14].

Although the literature concerning the preparation of porous materials through the chemical activation of bone char is scarce, there are several studies that demonstrate the suitability of this preparation method. For example, in a previous work [15] we determined that the acid treatment of bone char with either H_2SO_4 or H_3PO_4 increased the BET surface area by about 80%, compared to the sample prepared by physical activation only. Furthermore, the treatment with H_2SO_4 led to a dramatic increase in microporosity, up to 263%. The alkali treatment with K_2CO_3 and NaOH also proved to be effective [16], with an increase in S_{BET} of 45% and 39%, respectively, compared to the sample obtained by physical activation.

The knowledge of the mechanism involved in the activation of bone char and its impact on the properties of the material may be considerably beneficial to configure a material with the desired physicochemical properties. Several efforts have been made to understand the reactions that take place during the preparation of porous materials by chemical activation, using different carbonaceous precursors and activating agents. Guo and Lua [17] studied the chemical activation of oil-palm stone with H_2SO_4 and KOH. Lillo-Rodenas et al. [18,19] investigated the reactions occurring during the chemical activation of an anthracite with NaOH and KOH. Robau-Sánchez et al. [20] proposed a reaction mechanism for the activation of *Quercus agrifolia* char with KOH. Recently, we studied the reaction mechanism that takes place during the activation of sewage sludge with NaOH and K_2CO_3 [21].

The use of animal bones to prepare porous materials requires the development of specific reaction mechanisms, given its particular composition, with natural apatite being the main component. In this regard, the literature concerning the reaction mechanism that take place during the thermal activation of precursors derived from animal bones is scarce. Senneca [22] reported the products released during the thermal treatment of meat and bone meal. Although they used synthetic HAp, the study of Yasukawa et al. [23] is also of interest. These authors studied the thermal decomposition mechanism of HAp with TG-MS, focused on the release of H_2O and CO_2. To the best of the authors' knowledge, our previous studies are the only studies regarding the investigation of the activation mechanism that takes place during the chemical activation of bone char [15,16,24]. These studies are focused on the chemical activation of bone char with different reagents (NaOH, KOH, K_2CO_3, H_2SO_4, H_3PO_4) in an inert atmosphere.

The aim of this study is to extend the aforementioned investigation, in order to perform a comprehensive and detailed study of the activation mechanism for both pyrolysis and carbonization. For this purpose, thermogravimetric analysis coupled to mass spectrometry was used to investigate the gases released during the chemical activation of pork bone char with H_2SO_4 and K_2CO_3. These reagents were chosen based on their different nature (an acid and an alkali salt), as well as on the results of a previous investigation [2], which determined that both favour the development of porosity and effectively modify the pore size distribution.

Moreover, the study addresses the structural rearrangements and modifications in the chemical composition of the materials (measured by nitrogen adsorption-desorption, XRD, FTIR, SEM, elemental analysis and EDX) in terms of: (i) the heating atmosphere (inert or oxidizing), (ii) the highest treatment temperature, and (iii) the chemical reagent, H_2SO_4 and K_2CO_3. The results will be helpful to configure activation protocols for bioapatite-based materials with tailored physicochemical properties for use in specific fields.

2. Materials and methods

2.1. Production of bone char

Bone char (BC) was prepared from pork chop bones collected from a local butcher's shop. The preparation protocol was as follows: first, bones were cleaned from meat and cut into pieces of 2–5 cm. In order to remove meat and fat, prior to chemical activation bones were precarbonized in air flow (120 $cm^3\ min^{-1}$, corresponding to 8 min of residence time in furnace) at 500 ºC (heating rate of 10 ºC min^{-1}, hold 1 h), using a quartz tube furnace. Hereafter, the precarbonized sample will be referred as precursor.

The precursor was sieved and particles in the 0.09 – 0.25 mm size range were selected. The precursor was divided into three parts. Two were impregnated with either H_2SO_4 (S) or K_2CO_3 (K). The last sample was not further modified to be used as a reference (O). For the impregnation step, about 2 g of the precursor were placed into contact with 40 cm^3 of a solution containing the activating agent, using a ratio of 0.2 $mmol_{H2SO4}\ g^{-1}_{precursor}$ and 5 $mmol_{K2CO3}\ g^{-1}_{precursor}$ based on our previous experience [15,16]. The solutions were stirred at room temperature (20 ± 2 ºC) for 24 h, to ensure the access of the activating agent to the interior of the particles. The samples were then filtered, transferred to a convection oven and dried at 80 ºC for 24 h.

The impregnated samples were heated using operating conditions similar to those used during the precarbonization step. The highest treatment temperature (HTT) values were 600 and 800 ºC for inert –nitrogen– atmosphere, and 350 and 550 ºC for oxidizing –air– atmosphere. These values were selected based on the results of the TG-MS analysis of impregnated samples, as shown below. The prepared samples were coded according to the activating agent, the HTT value and the atmosphere: nitrogen (N) and air (A). For example, BCKA-550 refers to the sample of bone char prepared by impregnation with K_2CO_3 and activated in air at 550 ºC.

2.2. TG-MS study

Thermogravimetric analysis (TG) coupled to mass spectrometry (MS) was conducted with two aims: (i) investigate the reactions occurring during the thermal treatment of impregnated samples, and (ii) select the HTT. TG analysis was performed using a Setsys evolution (Setaram) thermal analyser. About 40 mg of impregnated samples were put into the ceramic crucible and heated in an inert (helium) or oxidizing (air) atmosphere from room temperature to 900 ºC, at a heating rate of 5 ºC min^{-1}. The exhaust gases were analysed on-line by a mass spectrometer (MKS, Cirrus LM99). The total pressure in the analysis chamber was 10^{-6} torr (1 torr = 133.32 Pa). The following compounds were monitored continuously: H_2 ($m/z = 2$), H_2O ($m/z = 18$), CO ($m/z = 12$) and CO_2 ($m/z = 44$). MS signals were normalized by dividing by sample mass.

2.3. Physicochemical characterization

The textural properties were determined by nitrogen adsorption/desorption at 77 K, using a porosimeter (ASAP 2010, Micromeritics). Prior to the measurements samples were dried and outgassed at 200 °C in a nitrogen flow for 15 h. BET surface area, pore area and pore volume were measured. The micropore surface and volume were obtained by t-plot method, whereas values in the mesopore and macropore ranges were determined based on the Barrett, Joyner & Halenda (BJH) method.

The crystalline structure was analysed by XRD using a Philips PW1710 diffractometer. X-ray powder diffraction patterns were collected by using a Philips X′pert PRO automatic diffractometer operating at 40 kV and 40 mA, in theta-theta configuration, secondary

monochromator with Cu-Kα radiation (λ = 1.5418 Å; 1 Å = 10^{-10} m) and a PIXcel solid state detector (active length in 2θ = 3.347°). The Rietveld method was used for microstructure analysis (profile refinement) and estimation of the unit cell parameters.

The surface properties of the materials were analysed by a scanning electron microscope (FEG-SEM Hitachi S-4800) and the quantitative analysis of the surface was performed by an EDX detector (Oxford Instrument X-Max). Fourier-transformed infrared (FTIR) spectra were collected using a Nicolet Protégé 460 device in the transmittance mode, over the 400–4000 cm^{-1} range with a resolution of 2 cm^{-1}. The KBr self-supported pellet technique was used to collect the spectra. The contents of carbon, hydrogen, and nitrogen were measured using a CHNS-O Euro EA3000 elemental analyser (EuroVector, Italy).

3. Results and discussion

3.1. Chemistry of the activation process

Fig. 1 shows the results of the thermogravimetric analysis of the impregnated precursor samples in both inert (helium) and oxidizing (air) atmospheres. The latter leads to a higher mass loss (17 wt% vs. 11–12 wt%). Moreover, the mass loss occurs at different temperature intervals depending on the atmosphere. Over the 50–130 °C range, mass loss is mainly ascribed to the release of adsorbed water, being around 1.4% and 1.9 wt%, for inert and air atmosphere, respectively. Over the 130–330 °C range, mass losses of around 1.7 and 2.2 wt%, respectively, take place, partly ascribed to the desorption of lattice water. Such values reflect the relatively important amount of the adsorbed and lattice water contained in the precursor. Between 330 and 550 °C, around 11 wt% of mass loss takes place in air atmosphere, being much lower (< 2%) in helium atmosphere. In this case, the mass loss occurs more progressively over the whole temperature range (130 – 900 °C), with an increase in mass loss rate above 600 °C. In the oxidative atmosphere, several pronounced peaks can be identified in the derivative TG profile.

These results reveal that different reactions and processes take place during the thermal activation of chemically impregnated samples. Thermal analysis was coupled to mass spectrometry in order to identify those reactions.

In order to propose a reaction mechanism for the activation process, the composition of the precursor (precarbonized bones) must be considered. XRD results (3.2.4. section) confirm that the precursor contains mainly bioapatite. Biological apatites differ chemically from stoichiometric HAp in that they contain additional elements substituted into the HAp lattice. Natural apatite can be expressed with the general formula $(Ca,M)_{10}(PO_4,Y)_6(OH,Z)_2$, where M represents monovalent (Na^+, K^+) or divalent (Mg^{2+}, Zn^{2+}, Sr^{2+}) cations that can substitute Ca^{2+} in the lattice, Y represents anions such as CO_3^{2-} or HPO_4^{2-} that can substitute PO_4^{3-}, and Z can be monovalent (F^-, Cl^-) or divalent (CO_3^{2-}) anions that substitute OH^- [11]. The carbon content in the precursor is noteworthy (9.2 wt%, Table 1). It is expected that the precarbonization of bones at 500 °C results in the incomplete removal of organic matter [25] and, moreover, carbon can be found in carbonate ions in bioapatite (detected by FTIR, 3.2.3 section). Biological apatites in bone minerals and consequently, bone char, contain significant amounts of carbonate ions (Cheung et al. [26] reported a content of CO_3^{2-} of 7–9 wt% in bone char). As previously discussed, bioapatite can host CO_3^{2-} ions in two possible anionic sites in the apatite lattice: (i) the OH^- position, forming type A carbonated apatite and (ii) the PO_4^{3-} location, forming type B carbonated apatite. Moreover, the simultaneous location of carbonates at both positions leads to a type AB carbonated apatite [11].

3.1.1. Samples activated in inert atmosphere

Fig. 2 depicts the evolution of mass spectrometric signals with temperature, corresponding to the main compounds released during the thermal activation of the precursor. Fig. 2a corresponds to the **precursor without impregnation**, activated in the inert (helium) atmosphere.

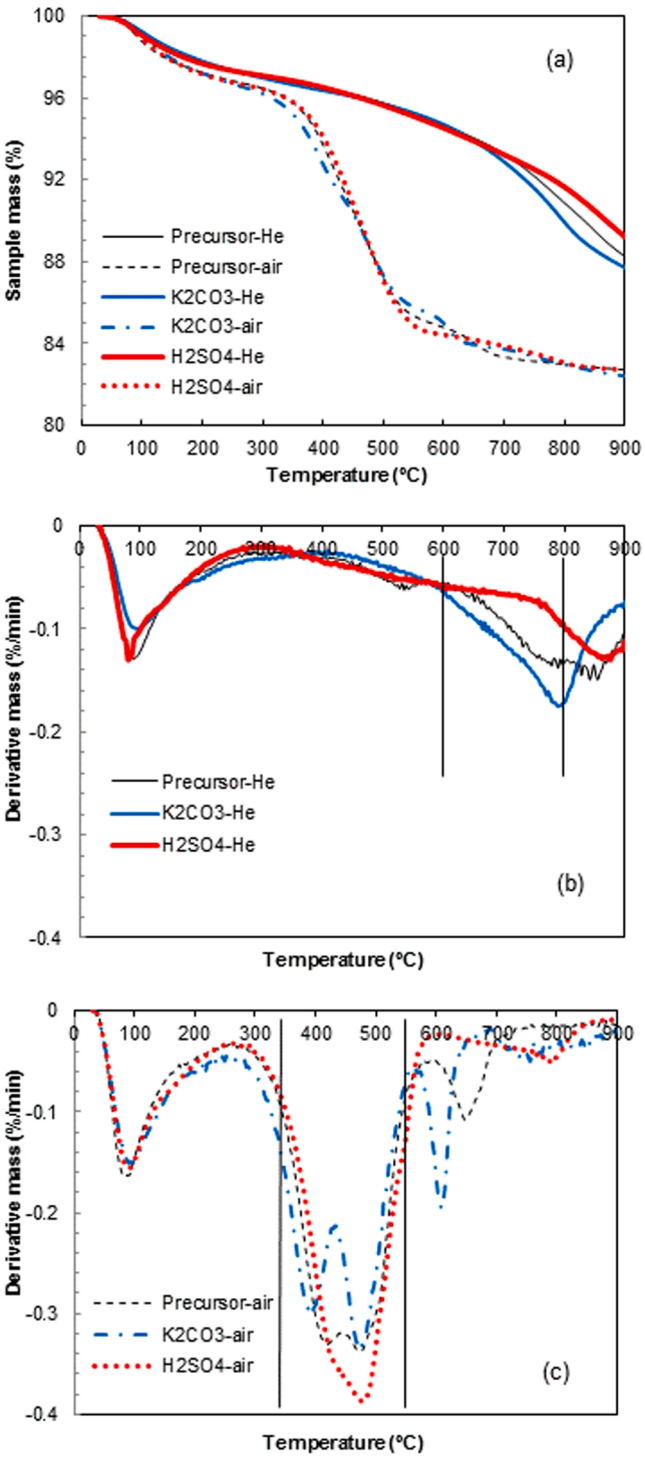

Fig. 1. Thermogravimetric analysis of the impregnated precursor. a) TG curves obtained in inert (He) and oxidizing (air) atmosphere; b) DTG curves obtained in inert (He) atmosphere; c) DTG curves obtained in oxidizing (air) atmosphere.

The mass loss up to 300 °C may be mainly attributed to the release of water. The signal of water shows the following features: (i) a main desorption peak, ascribed to the release of adsorbed water, (ii) a shoulder near 250 °C, attributed to the loss of lattice water [27] and (iii) a continuous release in the 300–900 °C range, assigned to the dehydroxylation of P-OH groups of bioapatite, which takes place mainly in the 300–700 °C range [28]:

$$2\ P{-}OH \leftrightarrow P{-}O{-}P + H_2O\ (g) \quad (1)$$

Table 1
Chemical composition of the prepared materials (wt%). H, C and N determined by elemental analysis. The rest of the elements measured by EDX. Ca/P given as molar ratio.

Sample	H	C	N	Ca	P	O	K	Na	Mg	Cl	S	Ca/P
Precursor	0.81	9.21	1.67	30.6	13.8	41.1	0.81	0.85	0.49	0.32	0.00	1.71
BCKA-350	1.39	4.64	1.19	31.0	13.8	44.2	1.45	0.61	0.54	0.15	0.00	1.74
BCKA-550	0.82	0.76	0.20	32.1	14.7	44.9	1.71	0.67	0.55	0.21	0.00	1.68
BCKN-600	1.04	0.31	< 0.1	34.4	16.2	41.1	1.42	0.63	0.6	0.21	0.00	1.64
BCKN-800	0.62	0.11	< 0.1	34.0	15.2	43.4	1.05	0.76	0.61	n/d	0.00	1.73
BCSA-350	1.04	6.70	1.49	29.1	13.4	42.9	n/d	0.5	0.39	0.15	0.07	1.68
BCSA-550	1.01	0.47	0.25	34.8	16.1	41.6	0.31	0.62	0.44	0.2	0.08	1.67
BCSN-600	0.60	0.37	0.13	34.4	15.7	41.4	0.45	0.75	0.46	0.21	0.16	1.70
BCSN-800	0.76	< 0.1	< 0.1	35.4	15.8	42.5	0.15	0.63	0.61	0.14	0.00	1.73

The release of CO_2 begins at 200 °C and progressively increases in the 200–700 °C range. The loss of CO_2 may be partially attributed to the reaction of CO_3^{2-} constituent of bone char with water (Eqs. (2) and (3)) [23].

$$CO_3^{2-} + H_2O \leftrightarrow HCO_3^- + OH^- \quad (2)$$

$$HCO_3^- \leftrightarrow CO_2 + OH^- \quad (3)$$

Furthermore, the thermal decomposition of carbonates above 600 °C (Eq. (4) is well documented [29,30]. The resulting oxide ions may undergo a subsequent hydration (Eq. (5)) [31]:

$$CO_3^{2-} \leftrightarrow CO_2 + O^{2-} \quad (4)$$

$$O^{2-} + H_2O \leftrightarrow 2\ OH^- \quad (5)$$

Of interest is that the mass loss at high temperature (above 600 °C, Fig. 1) coincides with the release of H_2 and CO. The release of H_2, starting at 500 °C, could be explained by the reaction of OH^- ions with the carbon constituent of the precursor, as proposed for other carbonaceous precursors [18,19,24]:

$$6\ OH^- + 2\ C \leftrightarrow 3\ H_2 + 2\ CO_3^{2-} \quad (6)$$

There are two sources of OH^- ions: (i) the P-OH functionalities of bioapatite, and (ii) the OH^- ions formed from carbonates (Eqs. (2)–(5)).

The release of CO, that takes place at temperatures above 600 °C, is likely due to the gasification of the carbon constituent of bone char. Two reactions could be involved: (i) the reverse Boudouard reaction, in which CO_2 reacts with carbon (Eq. (7)) [32], and (ii) water-gas reaction, in which water reacts with carbon (Eq. (8)) [33]:

$$CO_2 + C \leftrightarrow 2\ CO \quad (7)$$

$$H_2O + C \leftrightarrow CO + H_2 \quad (8)$$

Furthermore, the reaction mechanism described by Eqs. (9)-(10) should not be discarded, in which C acts as a reducing agent in the production of CO [34]. The required oxide is likely to be formed through the aforementioned thermal decomposition of CO_3^{2-} (Eq. 4).

$$O^{2-} + C \leftrightarrow CO \quad (9)$$

$$CO_3^{2-} + 2\ C \leftrightarrow 3CO \quad (10)$$

The shape of the signal of CO suggests the existence of overlapping processes. Moreover, the shoulder in the H_2 evolution profile, at around 850 °C, would support the occurrence of Eq. (8).

The **treatment with K_2CO_3** increases the intense weight loss above 600 °C, which takes place at lower temperature (Fig. 1b). As occurred for the pristine precursor, a significant signal of water is observed (Fig. 2c). The attenuation of the right shoulder and the diminished release of water in the 330–550 °C range indicate that the intensity of the steps of water desorption and dehydroxylation of P-OH groups is lessened. The signal of CO_2, attributed to the reaction of carbonates with water (Eqs. (2) and (3)) and to the thermal decomposition of carbonates (Eq. (4)), follows a similar profile to that in the pristine precursor. In this case, apart from the CO_3^{2-} constituent of bone char, the incorporated K_2CO_3 represents an additional source of carbonates, which are incorporated by ion exchange.

As previously explained, the mass loss at high temperature (above 600 °C) is associated with reactions that result in the release of H_2 and CO. The treatment with K_2CO_3 has an impact on the extent of those reactions, as confirmed by TG (Fig. 1). Regarding the release of CO (mainly attributed to the gasification of carbon constituent of bone char), the catalytic role of alkali metals (such as K, Mg, Na and Ca) is well known, for both the reverse Boudouard reaction and the gasification of carbon with steam (Eqs. (7)–(8)) [33,35], with K (incorporated by ion exchange) being the most active [35]. Furthermore, the incorporation of carbonate ions represents an additional source of carbon. Of interest is that the shape of the DTG curve (Fig. 1b) at high temperature (above 600 °C) is in concordance with the CO profile (Fig. 2), suggesting that the reactions that result in the release of CO (mainly carbon gasification reactions, Eqs. (7)–(8)) contribute to mass loss to a greater extent than those involving the release of H_2. Moreover, the impregnation with K_2CO_3 (an additional source of carbon) may increase the release of H_2, through the reaction of OH^- ions with carbon (Eq. (6)). Indeed, it is expected that the amount of OH^- ions will increase due to the reaction of the carbonates (Eqs. (2)–(5)).

As a consequence of the incorporation of K^+ ions (as evidenced by the data of Table 1), the occurrence of the reverse water gas shift reaction (RWGS) (Eq. (11)), reported in the pyrolysis of carbonaceous precursors [36,37], is also expected to take place. The role of K as promoter of the RWGS reaction is well established [38,39].

$$CO_2 + H_2 \leftrightarrow CO + H_2O \quad (11)$$

The **treatment with H_2SO_4** reduces the mass loss (i.e. 12%, Fig. 1a). The principal difference occurs in the high temperature range, where mass loss is the lowest and takes place at higher temperatures (Fig. 1b). Contrarily, as observed in the DTG plot, the mass loss in the 400–500 °C range increases slightly, as compared to the non-impregnated and the sample impregnated with K_2CO_3. It is hypothesized that the enhanced mass loss at medium temperature is related to the release of CO_2. The reaction of H^+ ions of the acid with carbonates would promote the formation of HCO_3^- ions (Eq. (12)), which would then be decomposed to CO_2 (Eq. (3)).

$$CO_3^{2-} + H^+ \leftrightarrow HCO_3^- \quad (12)$$

As previously mentioned, the mass loss above 600 °C is mainly related to the evolution of H_2 and CO (Fig. 2e). The release of H_2 is mostly attributed to Eq. (6), in which there is a reaction with OH^- ions and C. The lower availability of OH^- ions or C would result in a lower extent of this reaction.

Moreover, the previous treatment with H_2SO_4 could lead to specific reactions involving either carbon or CO_3^{2-} constituents of bone char (Eqs. (13–14)) [24]:

$$2\ H_2SO_4 + C \leftrightarrow CO_2 + 2\ SO_2 + 2\ H_2O \quad (13)$$

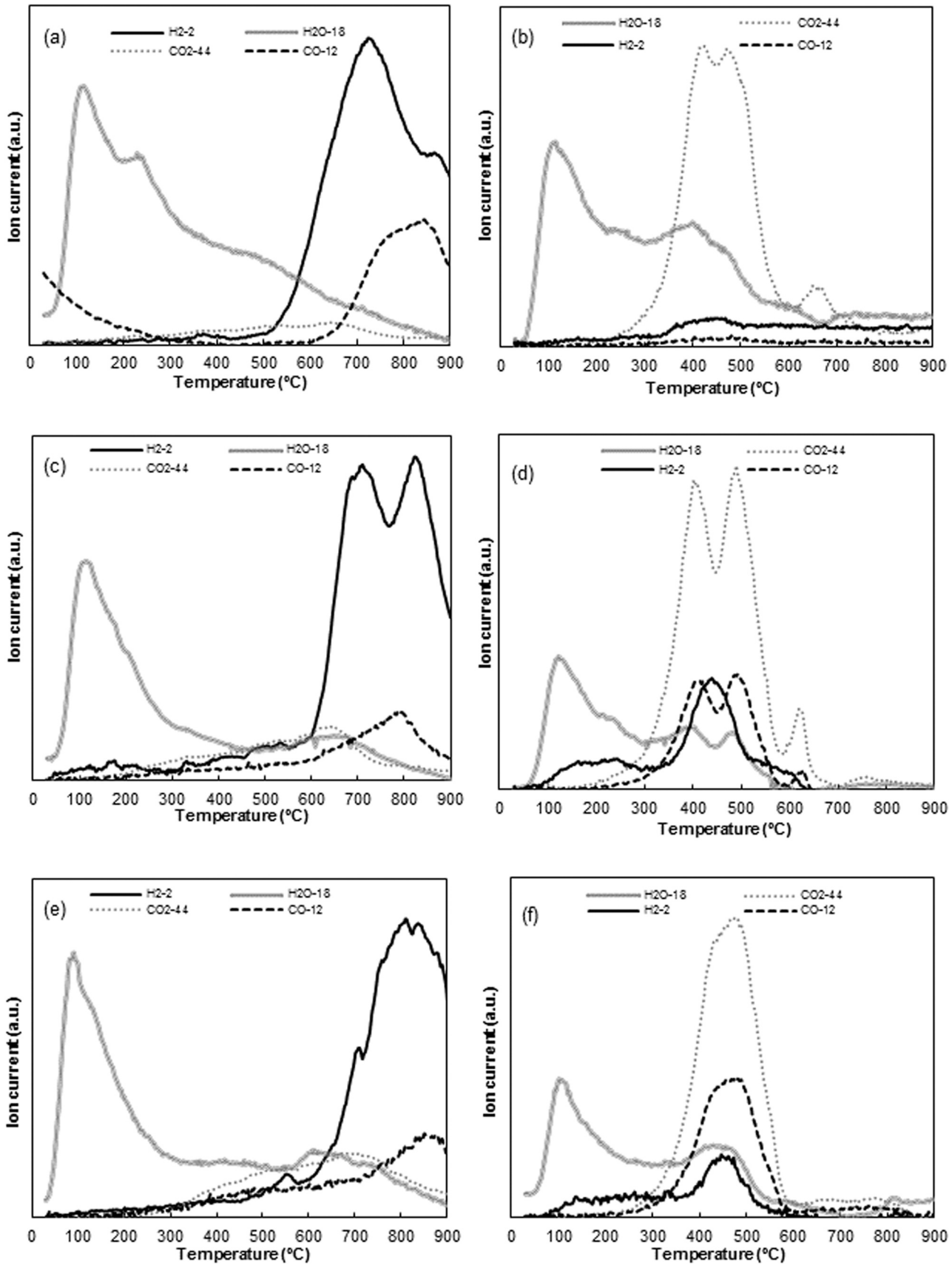

Fig. 2. Mass spectrometry data of the compounds released during the heat treatment. a) non-impregnated precursor in inert (He) atmosphere; b) non-impregnated precursor in oxidizing (air) atmosphere; c) precursor impregnated with K_2CO_3 in inert atmosphere; d) precursor impregnated with K_2CO_3 in oxidizing atmosphere; e) precursor impregnated with H_2SO_4 in inert atmosphere; f) precursor impregnated with H_2SO_4 in oxidizing atmosphere.

$$H_2SO_4 + CO_3^{2-} \leftrightarrow SO_4^{2-} + CO_2 + H_2O \quad (14)$$

Eqs. (13) and (14) would result in a lower amount of C and OH^- (formed from carbonates through Eqs. (2)–(5)). The fact that high amounts of CO_2 or H_2O are not released (according to the DTG, Fig. 1b) could be explained by the occurrence of both reactions during the impregnation step, before the thermal activation. Concerning CO (formed through Eqs. (7)-(10), the lower availability of carbon as a consequence of Eqs. (13) and (14) would also explain its lower release.

Furthermore, the treatment with H_2SO_4 could also result in the partial dissolution of bioapatite (regarded as a ramification of HAp) and the formation of calcium sulfate and calcium deficient bioapatite (Ca-deficient HAp is expressed with the formula $Ca_{10-x}(HPO_4)_x(PO_4)_{6-x}(OH)_{2-x}$) [23]. Nevertheless, the Ca/P ratios shown in Table 1 are close to the stoichiometric value of 1.67 of HAp, and do not show a decrease in BCS series, compared to the precursor and the BCK series. However, the incorporation of sulfate ions into bioapatite should also be taken into account. Indeed, it has been reported that SO_4^{2-} can substitute HPO_4^{2-} ion (both ions having the same valence and very similar ionic radius) [40]. The results of Table 1 reveal a small amount of S in BCS samples, whereas it is absent in the precursor and BCK samples. This process, that results in an increase of the Ca/P ratio, may offset the decrease in the ratio produced in the generation of calcium-deficient bioapatite.

Among the proposed reactions for impregnated and non-impregnated samples, the RWGS reaction takes place in gas phase and thus, does not contribute to generating porosity. In contrast, the reaction mechanisms that involve the gasification of constituents of bone char or incorporated species, are expected to have an impact on the textural properties of the materials.

3.1.2. *Samples activated in oxidizing atmosphere*

According to the DTG plot (Fig. 1c), the weight loss in the oxidizing environment takes place in three stages: low temperature (below 300 ºC), intermediate temperature (300–550 ºC) and high temperature (above 550 ºC). Among these intervals, the highest weight loss takes place across the intermediate temperature range (300–550 ºC).

Fig. 2b displays the main products released during the thermal activation of the **precursor**. The first stage of mass loss is mainly related to the release of water. As occurred with samples activated in inert atmosphere, the signal of water shows a principal peak, attributed to the desorption of adsorbed water, followed by a continuous release, ascribed to the elimination of lattice water, as well as the P-OH groups of apatite by dehydroxylation (Eq. (1)).

The most remarkable difference with respect to the inert atmosphere occurs in the medium temperature range, in which combustion reactions take place preferentially to other reactions:

$$C + O_2 \leftrightarrow CO_2 \quad (15)$$

$$2H + \frac{1}{2}O_2 \leftrightarrow H_2O \quad (16)$$

Two overlapping peaks can be distinguished in the CO_2 profile. It is hypothesized that these peaks are due to either the preferential combustion of carbon located near metals such as Ca, K, Mg, Na (Table 1) that act as catalysts for the combustion of carbonaceous species (peak at low temperature) [41,42] or to the heterogeneous nature of carbonaceous species (for example, carbon present in the structure of bioapatite as carbonates, and carbon present in the remaining organic matter). Additionally, there is a small peak of CO_2 with its maximum near 650 ºC, ascribed to the thermal decomposition of carbonates (Eq. (4)). The release of hydrogen and CO, that takes place in the intermediate temperature range, is almost negligible.

Fig. 2d shows the evolution of the main signals during the activation in air atmosphere of the precursor **impregnated with K_2CO_3**. The release of water and CO_2 follow a similar profile, compared to the non-impregnated precursor. Regarding the signal of CO_2, the two overlapping peaks appear more clearly defined in this case and the low temperature peak is slightly shifted to a lower temperature, which could be related to the aforementioned catalytic activity of the incorporated K metal (data in Table 1 clearly show that ion substitution takes place). The peak of CO_2 at high temperature, ascribed to the thermal decomposition of carbonates, is also better defined, owing to the amount of carbonates incorporated during the impregnation.

The principal differences are observed in the release of CO and H_2, almost absent in the non-impregnated precursor. Three possible pathways could be proposed for the signal of CO, that exhibits a similar shape to that of CO_2: (i) the incomplete combustion of carbon; (ii) the reverse water gas shift reaction (RWGS) (Eq.(11)), that produces CO and H_2O, promoted by the incorporated K; (iii) the gasification of carbon through the reverse Boudouard reaction (Eq. (7)) and through the water-gas reaction (Eq. (8)), catalyzed by K, as previously discussed.

Concerning the signal of H_2, a clear peak is observed at around 450 ºC, which is definitely much lower than the H_2 detection temperature in inert atmosphere (> 600 ºC). Apart from the water-gas reaction (Eq. (8)), the aforementioned reaction of OH^- ions with carbon (Eq. (6)) could be responsible for the release of H_2. The impregnation with K_2CO_3 may have an impact in both reactions: (i) the water-gas reaction is catalysed by K, and (ii) the incorporation of CO_3^{2-} in the position of phosphate would increase the amount of both carbon and OH^- ions, the latter formed through the reaction of carbonates (Eqs. (2)–(5)).

Finally, the evolution of the main products released during the activation of the sample **treated with H_2SO_4** is shown in Fig. 2f. The effect of the acid treatment is evidenced by the alteration of the released compounds in both the medium and high temperature range. As previously noted, the main mass loss event, which takes place in the intermediate temperature range, is shifted to higher temperatures by around 25 ºC, in comparison with non-impregnated sample (Fig. 1). The signal of CO_2, mainly ascribed to the combustion of carbon, suggests the existence of two overlapping peaks, but less defined than in the case of the sample impregnated with K_2CO_3. This behaviour could be partly attributed to the lower amount of metals that catalyse the combustion, such as K (Table 1). Moreover, the removal of part of the carbonaceous matter (both carbonates and the remaining organic matter) would results in less defined peaks of CO_2.

The signal of CO shows the same shape as that of CO_2. Moreover, the absence of the CO_2 peak at around 650 ºC supports the partial removal of carbonates by the acid (Eq. (14)). According to the FTIR results, discussed below (3.2.3. section, Table S1), all samples activated with H_2SO_4 show the characteristic peaks of carbonate, except for the sample activated at the highest temperature (BCSN-800). Thus, carbonates were not completely removed during the impregnation step, before the thermal treatment. The partial elimination of carbonates during the impregnation would explain the absence of the peak of CO_2 near 650 ºC. Indeed, the remaining carbonates would be completely removed by combustion, and there would be no carbonate available for removal by thermal decomposition.

The removal of the remaining organic matter and carbonates by the acid (Eqs. (13)-(14)) would also lead to a reduced amount of the H_2 released at intermediate temperature, formed from the reaction of OH^- and C (Eq. (6)). In fact, in addition to the lower amount of C available, there would be less OH^- ions available, as a consequence of: (i) the removal of carbonates, source of OH^- through Eqs. (2)–(5); and (ii) the partial dissolution of apatite, resulting in the formation of a cation deficient structure, which contains a lower amount of P-OH functionalities.

Except for the RWGS reaction, all the reaction mechanisms are expected to develop porosity, since they imply the gasification of constituents of bone char or incorporated species.

3.2. Characterization of bone chars

The impact of the aforementioned reaction mechanisms on the textural and chemical properties of the materials was investigated. Two levels of HTT were studied for each heating atmosphere, established on the basis of the TG-MS results (Fig. 1). The following HTT values were selected: 350 and 550 ºC for the oxidizing atmosphere, and 600 and 800 ºC for the inert atmosphere. The prepared materials were thoroughly characterised by elemental analysis, N_2 adsorption-desorption, XRD, SEM, EDX and FTIR analyses.

3.2.1. Chemical composition

Elemental and EDX analyses show the presence of abundant Ca, P, C and O, together with other elements such as K, Na, Mg and Cl (Table 1), reflecting the flexibility of natural apatites regarding the presence of different ions. Furthermore, as explained previously, the chemical treatment results in the incorporation of several species. The samples treated with K_2CO_3 show an increase in the amount of K, incorporated by ion exchange with Ca. It is also remarkable that the samples prepared by treatment with H_2SO_4 possess a small amount of S (absent in both the precursor and samples treated with K_2CO_3), reflecting the incorporation of SO_4^{2-} (substituting HPO_4^{2-}).

3.2.2. Textural properties and pore size distribution

The SEM images of the precursor and the samples treated in different atmosphere and temperature are presented in Fig. S1 (Supplementary material). Particles with flat and compact surfaces in the precursor are converted into coarse particles after the treatment. For the samples treated in air atmosphere, the surface texture becomes rougher and more porous after heating in the 350–550 ºC range. Regarding the thermal treatment in inert atmosphere, temperatures in the 600–800 ºC range result in the fragmentation of compact surfaces. It is observed that the bioapatite crystals are remarkably developed when increasing the HTT.

Table 2 summarizes the textural properties of bone char samples and Fig. 3 displays the pore size distribution (PSD). As observed, the textural properties vary significantly depending on the treatment applied (activating agent, atmosphere and temperature). These textural properties should be related to the extent of the aforementioned reactions and processes that generate porosity through the gasification of constituents of the precursor and species incorporated in the impregnation stage. Mainly: (i) the thermal decomposition and volatilization of the remaining organic matter; (ii) the desorption of adsorbed and lattice water; (iii) the dehydroxylation of apatite (Eq. (1)); (iv) the reaction of carbon with OH^- ions to produce H_2 (Eq. (6)); (v) the processes involving carbonates (transformation into OH^- ions and thermal decomposition) (Eqs. (2)–(5)); (vi) the gasification of carbon with either CO_2 or H_2O (Eqs. (7)–(8)); (vii) specific reactions involving the acid, such as the formation of HCO_3^- (Eq. (12)) and its subsequent decomposition (Eq. (3)) and the reaction of H_2SO_4 with carbon or carbonates (Eqs. (13)-(14)); (viii) the combustion of C and H (Eqs. (15)-(16)).

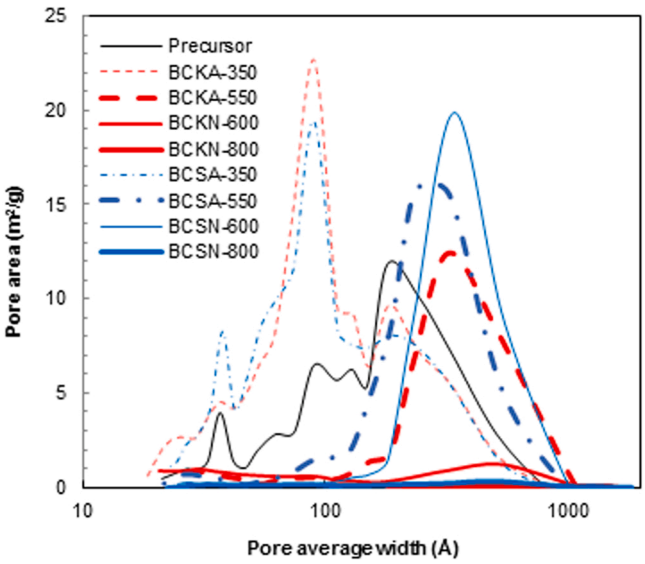

Fig. 3. Pore size distribution of the prepared materials.

When the activation is performed in **nitrogen atmosphere**, the highest activation temperature (800 ºC) results in a very aggressive treatment that leads to an almost complete destruction of the porous structure. The activation at lower temperature (600 ºC) has a different effect depending on the activating agent. The treatment with K_2CO_3 produces a material with a very low S_{BET} (17.0 m^2 g^{-1}) and porosity, whereas the material activated with H_2SO_4 better preserves the porous structure, with a S_{micro} similar to that of the precursor. Its most distinctive characteristic is the depletion of mesoporosity (Fig. 3), along with an increase of macroporosity, resulting in a higher average pore size (344 Å vs. 154 Å for the precursor).

On the other hand, the largest values of specific surface area are obtained **in oxidizing atmosphere** at HTT= 350 ºC (66.7% of increase for K_2CO_3 and 78.1% for H_2SO_4, compared to the precursor). As shown in Fig. 3, both activating agents result in a significant increase of small mesopores (d_p < 200 Å), along with a decrease of pores larger than that size. These results suggest that the combustion reactions that take place at intermediate temperature (Eqs. (15)-(16)) have a beneficial effect on the textural properties. In the case of the treatment with H_2SO_4, there is also a huge increase in S_{micro} (84.2%), whereas the impregnation with K_2CO_3 results in a decrease (30.9%). The selective development of microporosity through the impregnation with H_2SO_4 has been previously reported for other carbonaceous precursors based on animal bones [24]. This enhancement of microporosity may be attributed to the aforementioned specific reactions involving the acid (Eqs. (12)-(14)). Moreover, since these reactions result in a lower amount of carbon, carbonates and OH^- ions, a limitation in the extent of the reactions

Table 2
Textural properties of prepared samples of bone char and weight loss during the thermal treatment of impregnated samples.

Sample	S_{BET} (m^2 g^{-1})	S_{micro}[a] (m^2 g^{-1})	S_{ext}[a] (m^2 g^{-1})	V_p[b] (cm^3 g^{-1})	Pore size[b] (nm)	HAP crystal size (nm)	Muffle weight loss (wt%)
Precursor	63.4	10.0	53.4	0.3106	15.4	14.4	-
BCKA-350	105.7	6.9	98.8	0.3636	11.3	20.2	6.6
BCKA-550	38.5	8.9	29.6	0.2743	28.7	24.5	15.7
BCKN-600	17.0	4.3	12.6	0.0483	13.8	33.7	17.2
BCKN-800	1.2	1.2	0.0	0.0035	56.2	93.7	19.8
BCSA-350	112.9	18.4	94.5	0.3436	11.0	14.6	3.2
BCSA-550	56.6	11.3	45.3	0.3709	24.8	18.8	15.4
BCSN-600	42.0	9.5	32.5	0.3617	34.4	15.2	16.6
BCSN-800	6.2	2.4	3.7	0.0163	22.1	99.2	19.2

[a] t-plot method
[b] BJH method

involving those species could be expected, thus limiting the opening of the generated pores.

When the activation is performed in air atmosphere at higher temperature (HTT of 550 ºC), there is a considerable removal of the mesoporous structure below 100 Å (Fig. 3). This behaviour is accompanied with an increase of large mesopores ($d_p > \sim 250–300$ Å) and macropores, resulting in a higher average pore size. The greater extent of the combustion reactions could explain these results, since the higher amount of gases released could result in the opening of pores. The increase of microporosity with increasing HTT is noteworthy in the sample impregnated with K_2CO_3 (8.9 $m^2\ g^{-1}$ of S_{micro} at 550 ºC vs. 6.9 $m^2\ g^{-1}$ at 350 ºC). Contrarily, in the H_2SO_4 treated sample S_{micro} decreases with increasing HTT from 350 ºC to 550 ºC (18.4 vs. 11.3 $m^2\ g^{-1}$). Nevertheless, in the latter sample, the porosity in the micropore range is comparable to that of the precursor (10.0 $m^2\ g^{-1}$).

The effect of the atmosphere is noteworthy when BCKA-550 and BCSA-550 are compared to BCKN-600 and BCSN-600, respectively. The samples activated in air atmosphere possess much better textural properties across the whole pore range, suggesting the beneficial effect of the combustion reactions of carbon and hydrogen that take place preferentially to the other set of reactions. As previously discussed, this positive effect of the atmosphere can be maximized by performing the activation at lower temperature (350 ºC).

3.2.3. FTIR analysis

Fig. 4 displays the FTIR spectra of the precursor and the prepared samples of bone char. The spectra show the characteristic peaks of phosphates (phosphate stretching bands at 1040 and 960 cm^{-1}, the bending vibrations of these functional groups at 602 cm^{-1} and the antisymmetric stretching mode of phosphate at 1090 cm^{-1} [43]. The weak peak at 870 cm^{-1}, could be attributed to either the P-O stretching vibration [44] or the bending mode of carbonate groups [45].

Carbonates are observed at 1410 and 1460 cm^{-1} (C-O stretching mode), except for BCSN-800. Table S1 shows the ratio between the area of the peaks of carbonates and those of phosphates, in order to reflect the relative amount of carbonates of each sample. As expected, BCK samples possess a higher amount of carbonates than both the precursor and BCS samples, due to the incorporated carbonates. Moreover, the reaction of H_2SO_4 with carbonates (Eqs. (12) and (14)) would also explain the lower amount of BCS samples. In both series (BCK and BCS), the amount of carbonates decreases when temperature is increased, as a consequence of: (i) the thermal decomposition of carbonates (Eq. (4)), that takes place above 600 ºC; and (ii) the reaction of CO_3^{2-} with water (Eqs. (2)–(3)), in the 200–700 ºC temperature range. The same decreasing trend when temperature is increased is observed for the band near 1630 cm^{-1}, previously ascribed to carbonate ions [46]. Furthermore, the characteristic bands of organic matter are also observed for all samples (bands at 2850 and 2920 cm^{-1}), corresponding to the symmetric and asymmetric CH_2 stretching bands of organic matter [47].

The broad band at about 3400 cm^{-1} is commonly ascribed to –OH functional groups, and could be partially attributed to adsorbed water. As expected, there is a decrease in the intensity of this band when temperature is increased, in line with the above-mentioned reactions that involve OH^-, such as: (i) the elimination of the P-OH groups of HAP by dehydroxylation, Eq. (1); (ii) the reaction of OH^- ions with carbon to produce H_2, Eq. (6). Moreover, of interest is that the oxidant atmosphere results in a higher peak (for example, $A_{OH\text{-}}/A_{phosphate}$ is 0.75 for BCSA-550 and 0.57 for BCSN-600), suggesting that OH^- functional groups are generated from the reaction of oxygen with the hydrogen present (e.g. in the remaining organic matter).

3.2.4. XRD analysis

The XRD patterns of the prepared solids (Fig. 5) show diffraction peaks consistent with the apatite structure at 26.0°, 28.3°, 29.2, 32.0°, 32.4°, 33.1°, 34.3°, 40.0°, 46.9° and 49.7°. The refined lattice parameters (in Å, shown in Table 3) of the precursor (a = 9.40809, c = 6.8784)

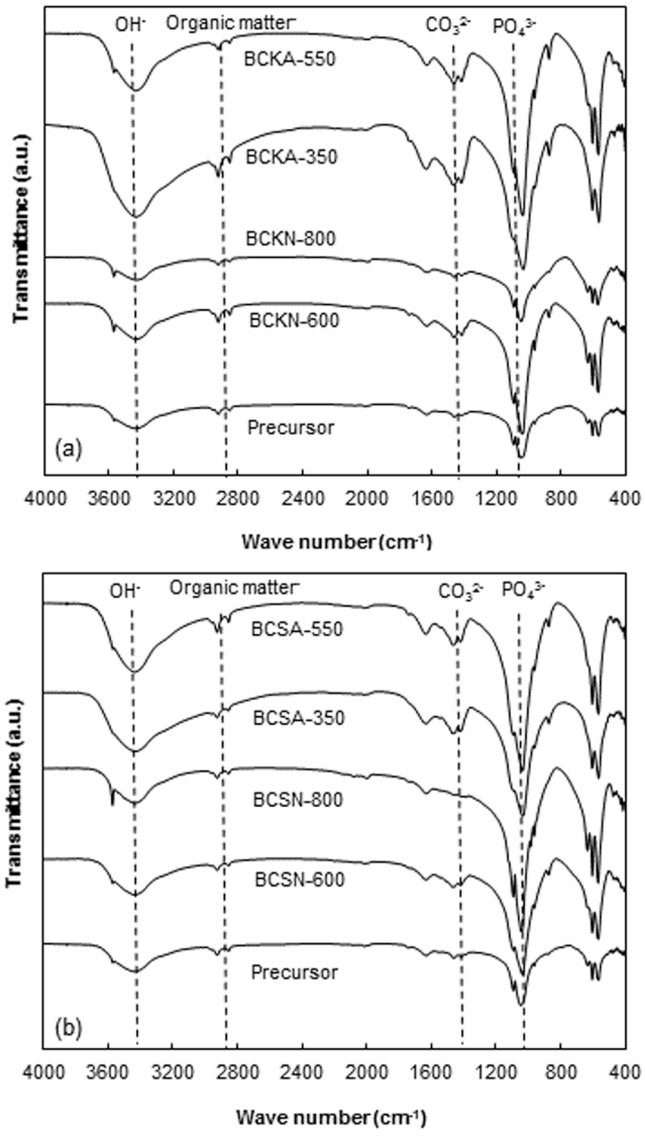

Fig. 4. FTIR spectra of the precursor and samples of bone char. a) samples prepared by impregnation with K_2CO_3; b) samples prepared by impregnation with H_2SO_4.

were smaller than those of pure hydroxyapatite (a = 9.4180, c= 6.884, ICDD 00–009–0432), reflecting the different chemical composition of biological apatites as a consequence of the substitution of different ions in the lattice. No other crystalline phases were observed in the analysed samples, except for BCSN-800, in which some traces of whitlockite ($Ca_{18}Mg_2H_2(PO_4)_{14}$, pdf 70–2064) are observed. The crystallinity of the materials increases with temperature, in concordance with the literature. Ooi et al. [48] reported that the thermal treatment above 600 ºC successfully eliminates the organic matter from bones, thus leading to an increase of the crystallinity. The XRD patterns show a higher degree of crystallinity for the samples impregnated with K_2CO_3, the effect being noteworthy for the samples activated at 600 ºC in inert atmosphere (BCKN-600 vs. BCSN-600). This lower crystallinity of BCS samples could be due to the fact that SO_4^{2-} ions were incorporated into the bioapatite lattice to some extent (as shown in Table 1) by ion exchange with HPO_4^-, in good concordance with the results of Toyama et al. [40].

The K_2CO_3-treated series follows the expected trend where the apatite crystal size increases with temperature (Table 2) [49]. However, for the H_2SO_4 treated samples, apatite crystallites of similar size (15–19 nm) are developed in the HTT = 350–600 ºC range. For both

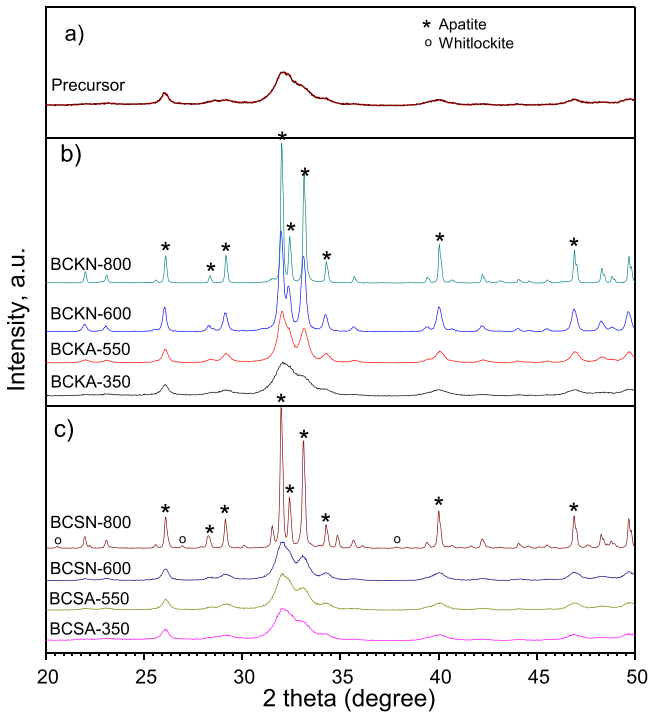

Fig. 5. XRD patterns of the precursor and samples of bone char. a) precursor; b) samples prepared by impregnation with K_2CO_3; c) samples prepared by impregnation with H_2SO_4.

Table 3
Lattice parameters obtained by Rietveld refinement.

	Lattice parameters				
	a, b	c	Delta a (%)	Delta c (%)	Cell volume, Å^3
Precursor	9.40809	6.8784			527.25
BCKA-350	9.4171	6.8991	0.10	0.30	529.852
BCKA-550	9.41439	6.8882	0.07	0.14	528.717
BCKN-600	9.41148	6.8844	0.04	0.09	528.094
BCKN-800	9.41336	6.8819	0.06	0.05	528.115
BCSA-350	9.43117	6.8968	0.25	0.27	531.264
BCSA-550	9.42198	6.8845	0.15	0.09	529.282
BCSN-600	9.42118	6.8831	0.14	0.07	529.082
BCSN-800	9.42663	6.8834	0.20	0.07	529.719

chemical agents, at the highest value of 800 ºC, the crystallite size increases significantly. In general terms, at similar HTT, larger apatite crystallites are formed in K_2CO_3 treated samples.

The lattice parameters *a* and *c* were calculated using the Rietveld method (Table 3). Lattice expansion is observed upon chemical activation, which suggests a possible incorporation of species into the apatite framework, along with other reactions or processes that can alter the structure of bioapatite. The expansion of the crystal lattice is different, depending on the activating agent used.

Regarding the activation with K_2CO_3, the expansion of lattice parameter *c* is higher (two or three times) than that of parameter *a*, with the exception of BCKN-800 (for which a lower and more equilibrated increase of *a* and *c* parameters is observed). Among the processes that result in an expansion of the crystal lattice, the ionic exchange of the incorporated K^+ and CO_3^{2-} ions may play an important role. Indeed, the ionic radii of K^+ and CO_3^{2-} are larger than those of Ca^{2+}, and OH^-, respectively. It is remarkable that the expansion in both *a* and *c* lattice dimensions generally decreases with temperature. This effect would be a result of processes that cause the contraction of the crystal lattice, such as the dehydroxylation of bioapatite (Eq. (1)) and the transformation of carbonates into OH^- ions (Eqs. (2)–(5)). Moreover, it has been reported that the loss of lattice water causes a contraction in the *a*-lattice dimension [50].

By contrast, the H_2SO_4 treatment causes a more marked expansion in the *a* axis (with the exception of BCSA-350, with a balanced increase in both parameters), suggesting that the activation with H_2SO_4 alters the crystalline structure through a different mechanism. Regarding the ion exchange, as explained in 3.1.1 section, SO_4^{2-} may be incorporated into the bioapatite structure, substituting HPO_4^- (as reported by Toyama et al. [40]). Nevertheless, since the ionic radii of both SO_4^{2-} and HPO_4^- are very similar, this ion exchange would not result in the expansion of the crystal lattice. Among the specific reactions promoted by the acid that could result in the expansion of the lattice, the incorporation of H^+ ions into the apatite structure through the formation of HCO_3^- ions should be highlighted (Eq. (12)).

4. Conclusions

The activation mechanism proposed for the precursor in inert atmosphere (pyrolysis) includes: (i) the thermal decomposition and volatilization of organic matter; (ii) the desorption of adsorbed and lattice water; (iii) the dehydroxylation of apatite; (iv) the reaction of carbon with OH^- ions to produce H_2; (v) the processes involving carbonates (transformation into OH^- ions and thermal decomposition); (vi) the gasification of carbon with either CO_2 or H_2O and (vii) the reverse water gas shift reaction. When the oxidizing atmosphere is used (carbonization), the combustion of both C and H - which takes place preferentially - must be added to the reaction scheme.

The effect of K_2CO_3 on the activation is probably a consequence of the incorporation of both K^+ and CO_3^{2-} ions into the bioapatite lattice by ion exchange. K^+ is a catalyst for the following reactions: (i) the combustion of C and H; (ii) the gasification of carbon with either CO_2 or H_2O and (iii) the RWGS reaction. Moreover, the increase of the amount of CO_3^{2-} results in a higher extent of the reactions involving carbonates and/or OH^- ions (formed from carbonates). Regarding H_2SO_4, it is hypothesized that its effect is mainly a consequence of specific reactions: (i) the reaction of H_2SO_4 with carbon or carbonates and (ii) the formation of HCO_3^- and its subsequent decomposition. Since these reactions result in a lower amount of carbon, carbonates and OH^- ions, a limitation in the extent of the aforementioned reactions involving those species could be expected.

The best textural properties are obtained in oxidizing atmosphere at 350 ºC, reflecting the beneficial effect of the combustion reactions at intermediate temperature. The economic benefit of using a moderate temperature should be highlighted. Between both reagents, H_2SO_4 provides better results in S_{BET} and, furthermore, leads to a selective development of microporosity. This enhancement in microporosity may be ascribed to either the occurrence of the aforementioned reaction involving the acid and/or to the limitation in the extent of other reactions – thus limiting the opening of the generated pores. The FTIR results suggest that the oxidizing atmosphere is involved in the generation of OH^- functional groups. The XRD results reveal an alteration in the structure of bioapatite: K_2CO_3 leads to a more marked expansion in the *c* axis, whereas for H_2SO_4 the expansion is higher in the *a* axis.

These results demonstrate the feasibility of configuring thermochemical activation protocols (choosing the most suitable activating agent, atmosphere or treatment temperature) to tailor the physicochemical properties of bioapatite-based materials, for use in specific fields.

CRediT authorship contribution statement

I. Sierra: Formal analysis, Writing – original draft. **José L. Ayastuy:** Conceptualization, Funding acquisition, Investigation. **Miguel A. Gutiérrez-Ortiz:** Funding acquisition, Supervision. **U. Iriarte-Velasco:** Conceptualization, Funding acquisition, Investigation, Writing – review & editing.

Declaration of Competing Interest

The authors declare that they have no known competing financial interests or personal relationships that could have appeared to influence the work reported in this paper.

Data Availability

Data will be made available on request.

Acknowledgements

This work was supported by the Basque Government (GV-2018–00038). The authors wish to express their gratitude for the technical and human support provided by SGIker of the UPV/EHU.

Appendix A. Supporting information

Supplementary data associated with this article can be found in the online version at doi:10.1016/j.jaap.2023.105973.

References

[1] N.I. Agbeboh, I.O. Oladele, O.O. Daramola, A.A. Adediran, O.O. Olasukanmi, M. O. Tanimola, Environmentally sustainable processes for the synthesis of hydroxyapatite, Heliyon 6 (2020), e03765.
[2] U. Iriarte-Velasco, I. Sierra, E.A. Cepeda, R. Bravo, J.L. Ayastuy, Methylene blue adsorption by chemically activated waste pork bones, Color. Technol. 131 (2015) 322–332.
[3] A. Rezaee, G. Ghanizadeh, G. Behzadiyannejad, A. Yazdanbakhsh, S.D. Siyadat, Adsorption of endotoxin from aqueous solution using bone char, Bull. Environ. Contam. Toxicol. 82 (2009) 732–737.
[4] M. Ferri, S. Campisi, M. Scavini, C. Evangelisti, P. Carniti, A. Gervasini, In-depth study of the mechanism of heavy metal trapping on the surface of hydroxyapatite, Appl. Surf. Sci. 475 (2019) 397–409.
[5] Y. Yang, C. Sun, B. Lin, Q. Huang, Surface modified and activated waste bone char for rapid and efficient VOCs adsorption, Chemosphere 256 (2020), 127054.
[6] A. Fihri, C. Len, R.S. Varma, A. Solhy, Hydroxyapatite: a review of syntheses, structure and applications in heterogeneous catalysis, Coord. Chem. Rev. 347 (2017) 48–76.
[7] P.A. Goodman, H. Li, Y. Gao, Y.F. Lu, J.D. Stenger-Smith, J. Redepenning, Preparation and characterization of high surface area, high porosity carbon monoliths from pyrolyzed bovine bone and their performance as supercapacitor electrodes, Carbon 55 (2013) 291–298.
[8] J. Cao, R. Lian, X. Jiang, Magnesium and fluoride doped hydroxyapatite coatings grown by pulsed laser deposition for promoting titanium implant cytocompatibility, Appl. Surf. Sci. 515 (2020), 146069.
[9] N. Mohan, R. Palangadan, F.B. Fernandez, H. Varma, Preparation of hydroxyapatite porous scaffold from a 'coral-like' synthetic inorganic precursor for use as a bone substitute and a drug delivery vehicle, Mater. Sci. Eng.: C. 92 (2018) 329–337.
[10] M. Gruselle, Apatites: a new family of catalysts in organic synthesis, J. Organomet. Chem. 793 (2015) 93–101.
[11] S. Bee, Z.A.A. Hamid, Hydroxyapatite derived from food industry bio-wastes: Syntheses, properties and its potential multifunctional applications, Ceram. Int. 46 (2020) 17149–17175.
[12] A. Benítez, J. Amaro-Gahete, Y. Chien, Á. Caballero, J. Morales, D. Brandell, Recent advances in lithium-sulfur batteries using biomass-derived carbons as sulfur host, Renew. Sustain. Energy Rev. 154 (2022), 111783.
[13] Z. Heidarinejad, M.H. Dehghani, M. Heidari, G. Javedan, I. Ali, M. Sillanpää, Methods for preparation and activation of activated carbon: a review, Environ. Chem. Lett. 18 (2020) 393–415.
[14] P. Gonzalez-Garcia, Activated carbon from lignocellulosics precursors: a review of the synthesis methods, characterization techniques and applications, Renew. Sustain. Energy Rev. 82 (2018) 1393–1414.
[15] U. Iriarte-Velasco, I. Sierra, L. Zudaire, J.L. Ayastuy, Preparation of a porous biochar from the acid activation of pork bones, Food Bioprod. Process. 98 (2016) 341–353.
[16] U. Iriarte-Velasco, I. Sierra, L. Zudaire, J.L. Ayastuy, Conversion of waste animal bones into porous hydroxyapatite by alkaline treatment: effect of the impregnation ratio and investigation of the activation mechanism, J. Mater. Sci. 50 (2015) 7568–7582.
[17] J. Guo, A.C. Lua, Textural and chemical characterisations of activated carbon prepared from oil-palm stone with H_2SO_4 and KOH impregnation, Microporous Mesoporous Mater. 32 (1999) 111–117.
[18] M.A. Lillo-Ródenas, D. Cazorla-Amorós, A. Linares-Solano, Understanding chemical reactions between carbons and NaOH and KOH: an insight into the chemical activation mechanism, Carbon 41 (2003) 267–275.
[19] M.A. Lillo-Ródenas, J. Juan-Juan, D. Cazorla-Amorós, A. Linares-Solano, About reactions occurring during chemical activation with hydroxides, Carbon 42 (2004) 1371–1375.
[20] A. Robau-Sánchez, A. Aguilar-Elguézabal, J. Aguilar-Pliego, Chemical activation of Quercus agrifolia char using KOH: Evidence of cyanide presence, Microporous Mesoporous Mater. 85 (2005) 331–339.
[21] I. Sierra, U. Iriarte-Velasco, J.L. Ayastuy, A.T. Aguayo, Production of magnetic sewage sludge biochar: investigation of the activation mechanism and effect of the activating agent and temperature, BiomassConvers. Biorefin. (2022).
[22] O. Senneca, Characterisation of meat and bone mill for coal co-firing, Fuel 87 (2008) 3262–3270.
[23] A. Yasukawa, K. Kandori, T. Ishikawa, TPD-TG-MS study of carbonate calcium hydroxyapatite particles, Calcif. Tissue Int. 72 (2003) 243–250.
[24] U. Iriarte-Velasco, J.L. Ayastuy, L. Zudaire, I. Sierra, An insight into the reactions occurring during the chemical activation of bone char, Chem. Eng. J. 251 (2014) 217–227.
[25] Q. Liu, S. Huang, J.P. Matinlinna, Z. Chen, H. Pan, Insight into biological apatite: physiochemical properties and preparation approaches, BioMed. Res. Int. 2013 (2013), 929748.
[26] C.W. Cheung, C.K. Chan, J.F. Porter, G. McKay, Combined diffusion model for the sorption of cadmium, copper, and zinc ions onto bone char, Environ. Sci. Technol. 35 (2001) 1511–1522.
[27] R. Chakraborty, S. Bepari, A. Banerjee, Application of calcined waste fish (Labeo rohita) scale as low-cost heterogeneous catalyst for biodiesel synthesis, Bioresour. Technol. 102 (2011) 3610–3618.
[28] H. Tanaka, T. Watanabe, M. Chikazawa, FTIR and TPD studies on the adsorption of pyridine, n-butylamineand acetic acid on calcium hydroxyapatite, J. Chem. Soc. Faraday Trans. 93 (1997) 4377–4381.
[29] Y. Wang, W.J. Thomson, The effect of sample preparation on the thermal decomposition of $CaCO_3$, Thermochim. Acta 255 (1995) 383–390.
[30] R.L. Lehman, J.S. Gentry, N.G. Glumac, Thermal stability of potassium carbonate near its melting point, Thermochim. Acta 316 (1998) 1–9.
[31] C. Combes, S. Cazalbou, C. Rey, Apatite biominerals, Minerals 6 (2016).
[32] C.G. Soni, Z. Wang, A.K. Dalai, T. Pugsley, T. Fonstad, Hydrogen production via gasification of meat and bone meal in two-stage fixed bed reactor system, Fuel 88 (2009) 920–925.
[33] H. Ren, Y. Zhang, Y. Fang, Y. Wang, Co-gasification behavior of meat and bone meal char and coal char, Fuel Process Technol. 92 (2011) 298–307.
[34] M. Hunsom, C. Autthanit, Adsorptive purification of crude glycerol by sewage sludge-derived activated carbon prepared by chemical activation with H_3PO_4, K_2CO_3 and KOH, Chem. Eng. J. 229 (2013) 334–343.
[35] C.K. Acharya, F. Jiang, C. Liao, P. Fitzgerald, K.S. Vecchio, R.J. Cattolica, Tar and CO_2 removal from simulated producer gas with activated carbon and charcoal, Fuel Process Technol. 106 (2013) 201–208.
[36] W. Chen, B. Lin, Hydrogen and synthesis gas production from activated carbon and steam via reusing carbon dioxide, Appl. Energy 101 (2013) 551–559.
[37] B. Prabowo, K. Umeki, M. Yan, M.R. Nakamura, M.J. Castaldi, K. Yoshikawa, CO_2–steam mixture for direct and indirect gasification of rice straw in a downdraft gasifier: Laboratory-scale experiments and performance prediction, Appl. Energy 113 (2014) 670–679.
[38] A. Bansode, B. Tidona, P.R. von Rohr, A. Urakawa, Impact of K and Ba promoters on CO_2 hydrogenation over Cu/Al_2O_3 catalysts at high pressure, Catal. Sci. Technol. 3 (2013) 767–778.
[39] C. Chen, W. Cheng, S. Lin, Study of reverse water gas shift reaction by TPD, TPR and CO_2 hydrogenation over potassium-promoted Cu/SiO_2 catalyst, Appl. Catal. A Gen. 238 (2003) 55–67.
[40] T. Toyama, S. Kameda, N. Nishimiya, Synthesis of Sulfate-ion-substituted Hydroxyapatite from Amorphous Calcium Phosphate, Bioceram. Dev. Appl. S1 (2013) 011.
[41] A. Carvalho, M. Rabaçal, M. Costa, M.U. Alzueta, M. Abián, Effects of potassium and calcium on the early stages of combustion of single biomass particles, Fuel 209 (2017) 787–794.
[42] M. Safar, B. Lin, W. Chen, D. Langauer, J. Chang, H. Raclavska, A. Pétrissans, P. Rousset, M. Pétrissans, Catalytic effects of potassium on biomass pyrolysis, combustion and torrefaction, Appl. Energy 235 (2019) 346–355.
[43] J. Reyes-Gasga, E.L. Martínez-Piñeiro, G. Rodríguez-Álvarez, G.E. Tiznado-Orozco, R. García-García, E.F. Brès, XRD and FTIR crystallinity indices in sound human tooth enamel and synthetic hydroxyapatite, Mater. Sci. Eng.: C. 33 (2013) 4568–4574.
[44] K.K. Bamzai, S. Suri, V. Singh, Synthesis, characterization, thermal and dielectric properties of pure and cadmium doped calcium hydrogen phosphate, Mater. Chem. Phys. 135 (2012) 158–167.
[45] M.A. Giardina, M.A. Fanovich, Synthesis of nanocrystalline hydroxyapatite from $Ca(OH)_2$ and H_3PO_4 assisted by ultrasonic irradiation, Ceram. Int. 36 (2010) 1961–1969.
[46] J.C. Merry, I.R. Gibson, S.M. Best, W. Bonfield, Synthesis and characterization of carbonate hydroxyapatite, J. Mater. Sci. Mater. Med 9 (1998) 779–783.
[47] M.M. Figueiredo, Characterization of Bone and Bone-Based Graft Materials Using FTIR Spectroscopy, in: J.A.F. Gamelas (Ed.), Infrared Spectroscopy, IntechOpen Rijeka, 2012 pp. Ch. 18.

[48] C.Y. Ooi, M. Hamdi, S. Ramesh, Properties of hydroxyapatite produced by annealing of bovine bone, Ceram. Int. 33 (2007) 1171–1177.
[49] W. Khoo, F.M. Nor, H. Ardhyananta, D. Kurniawan, Preparation of natural hydroxyapatite from bovine femur bones using calcination at various temperatures, Procedia Manuf. 2 (2015) 196–201.
[50] K. Tõnsuaadu, K.A. Gross, L. Plūduma, M. Veiderma, A review on the thermal stability of calcium apatites, J. Therm. Anal. Calorim. 110 (2012) 647–659.